Non-Fourier heat conduction in a single-walled carbon nanotube: Classical molecular dynamics simulations

Junichiro Shiomi and Shigeo Maruyama*

Department of Mechanical Engineering, The University of Tokyo
7-3-1 Hongo, Bunkyo-ku, Tokyo 113-8656, Japan

Non-stationary heat conduction in a single-walled carbon nanotube was investigated by applying a local heat pulse with duration of sub-picoseconds. The investigation was based on classical molecular dynamics simulations, where the heat pulse was generated as coherent fluctuations by connecting a thermostat to the local cell for a short duration. The heat conduction through the nanotube was observed in terms of spatio-temporal temperature profiles. Results of the simulations exhibit non-Fourier heat conduction where the distinct amount of heat is transported in a wavelike form. The geometry of carbon nanotubes allows us to observe such a phenomenon in the actual scale of the material. The resulting spatio-temporal profile was compared with the available macroscopic equations so called non-Fourier heat conduction equations in order to investigate the applicability of the phenomenological models to the quasi-one-dimensional system. The conventional hyperbolic diffusion equation fails to predict the heat conduction due to the lack of local diffusion. It is shown that this can be remedied by adopting the model with dual relaxation time. Further modal analyses using wavelet transformations reveal a significant contribution of the optical phonon modes to the observed wavelike heat conduction. The result suggests that, in carbon nanotubes with finite length where the long wavelength acoustic phonons behave ballistic, even optical phonons can play a major role in the non-Fourier heat conduction.

PACS numbers: 61.46.Fg, 65.80.+n, 67.40.Pm

*Corresponding author: Tel & Fax: +81-3-5800-6983.
E-mail address: maruyama@photon.t.u-tokyo.ac.jp

1. INTRODUCTION

The deviation of non-stationary heat conduction from the fully diffusive Fourier's law description is known to become significant when time and length scales of the system are within certain temporal and spatial windows of relaxation [1]. The derivations of models for the non-Fourier heat conduction usually take either microscopic (phonon) or macroscopic (continuum) approach, but reach similar expressions that suggest the collective phonons or heat propagating in a wavelike form with a certain speed.

In a typical macroscopic description, a well-known model of heat wave propagation was formulated by Cattaneo and Vernotte [2, 3], which gives rise to the conventional hyperbolic energy equation,

$$\tau \frac{\partial^2 T}{\partial t^2} + \frac{\partial T}{\partial t} = \alpha \nabla^2 T , \qquad (1)$$

where heat is conducted as a wave whose amplitude decays with an effective relaxation time τ. Here, θ and α are temperature and thermal diffusivity, $\lambda / \rho c_v$. The flexibility of the wave propagation models can be tuned by taking multiple timescales into account. For example, propagation of heat with two relaxation timescales can be expressed as

$$\tau_q \frac{\partial^2 T}{\partial t^2} + \frac{\partial T}{\partial t} = \alpha \left(\nabla^2 T + \tau_\theta \frac{\partial}{\partial t} \nabla^2 T \right). \qquad (2)$$

The expression can be derived by expanding the heat flux and temperature gradient with different relaxation times τ_q and τ_θ respectively [4]. At the limit of τ_θ=0, the expression is reduced to Eq. (1). In contrast to the hyperbolic equation, with the additional final term expressing the local diffusion of the heat wave, Eq. (2) exhibits various types of non-stationary heat conduction; wavy, wavelike, and fully diffusive heat conduction depending on the relaxation parameters [5].

In terms of phonons, the heat wave can be considered to be the extension of the second sound, i.e. the sound propagation in phonon gas, but with relaxation and dissipation due to the excess Umklapp phonon scattering or other momentum losing processes [6]. Starting from the phonon Boltzmann transport equation, one can derive a similar expression as Eq. (2) involving two relaxation times of normal (momentum conserved) and Umklapp (momentum non-conserved) scattering, τ_N and τ_R [1,7].

$$\frac{\partial^2 T}{\partial t^2} + \frac{1}{\tau_R}\frac{\partial T}{\partial t} = \frac{c^2}{3}\nabla^2 T + \frac{3}{5}\tau_N c^2 \frac{\partial}{\partial t}\nabla^2 T, \qquad (3)$$

where c is the group velocity. Eq. (3) can be reduced to Eq. (2) through the relations; $\tau_q = \tau_R$, $\lambda = \rho c_v \alpha = \rho c_v c^2 \tau_R / 3$ and $\tau_\theta = 9\tau_N / 5$. Although the microscopic relation is consistent with the macroscopic counterpart, there are still remaining issues such as the relevancy of the condition τ_N=0 for Eq. (3) to reduce to the hyperbolic equation where the heat conduction would be characterized solely by τ_R, or the revisiting conceptual problem of heat propagation at infinite speed due to the local diffusion term in Eq. (2) [1]. Therefore, the connection between the microscopic description of wavelike heat conduction and the phenomenological macroscopic relations has not been completely established.

The study of heat wave has a long history as the vast early literature was reviewed by [1]. One of the successes in the previous works was the prediction and demonstration of the second sound. Furthermore, theoretical analyses of second-sound mode under linear approximation revealed that the speed of second sound in the isotropic three-dimensional material is $c = c_D / \sqrt{3}$ [8, 9], where c_D is the Debye speed of sound $(c_D = \partial\omega/\partial k = \omega/k)$. While most of the theories are limited to systems with weak nonlinearity, Tsai and MacDonald [10] were the first to perform molecular dynamics (MD) simulations to examine the propagation of a heat wave under strongly anharmonic conditions. Despite the fundamental difference from the linear theories, they showed that the observed phenomenon is strikingly similar to the ones by linear analyses. Later, Volz et.al [11] performed MD simulations of thermally perturbed solid argon and compared the results with the Cattaneo-Vernotte equation. The temporal evolutions of thermal energy exhibited large discrepancy within the time duration of relaxation.

While the non-Fourier heat conduction has caught many early attentions as a controversial phenomenon of fundamental physics in heat transfer, the practical importance of this classical problem has been recently enhanced due to the development of high speed laser techniques and nano-scale materials. In the situations where sub-pico seconds heat pulse is generated by ultra-fast pulsed lasers on nanomaterials, the finite relaxation time of the heat transport can have a significant impact on the overall heat transfer [12]. In the currently work, we take an extreme case by applying a local heat pulse with duration of sub-picoseconds to a single-walled carbon nanotube (SWNT). By using classical molecular dynamics simulations, we investigate the non-Fourier heat conduction of an SWNT under anharmonic effects. Phonons of a pure SWNT are expected to possess a long mean free path due to the quasi-one-dimensional nature and the absence of defective and boundary scatterings, hence impact of such non-Fourier heat conduction may be significant in the real scale.

In the current paper, we first demonstrate the observation of heat waves in an SWNT. Then we validate the relevancy of above mentioned different macroscopic expressions in the nanoscale system. Finally, the collective phonon waves are further characterized by modal analyses and the active roles of optical phonons are demonstrated.

2. MOLECULAR DYNAMICS SIMULATIONS

The molecular dynamics simulations were performed for a 25 nm long (5,5) single-walled carbon nanotube subjected to periodic boundary conditions. The carbon-carbon interactions were expressed by the Brenner potential [13] with the simplified form [14] where the total potential energy of the system is expressed as,

$$E = \sum_i \sum_{j(i<j)} \left[V_R(r_{ij}) - B^*_{ij} V_A(r_{ij}) \right]. \qquad (4)$$

Here, $V_R(r)$ and $V_A(r)$ are repulsive and attractive force terms which take the Morse type form with a certain cut-off function. B^*_{ij} represents the effect of the bonding order parameters. As for the potential parameters, we employ the set that was shown to

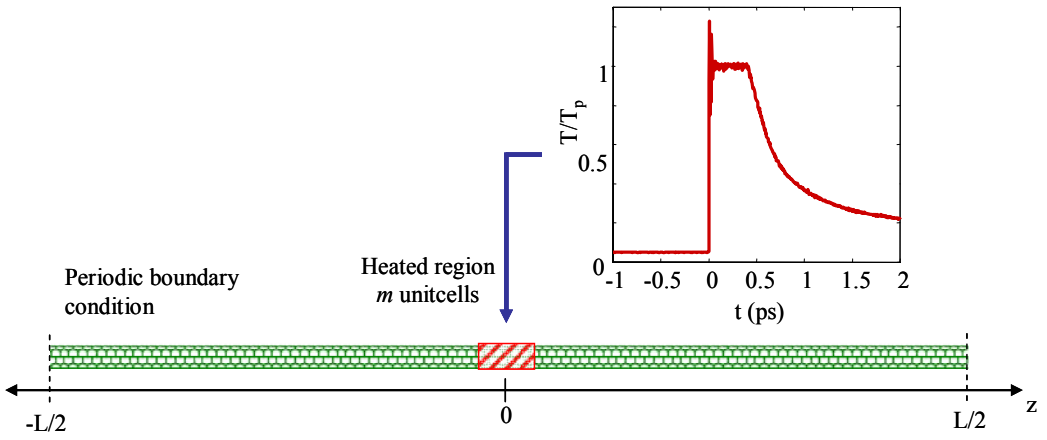

Fig. 1. A (5,5)-SWNT subjected to a heat pulse on a local m unit-cells located at the center of the periodic computational domain. The inset denotes the temperature response of the local heat region to the Nose-Hoover thermostat with relaxation time of 4 fs. Typical values of m and L are 6 and 25nm, respectively.

reproduce the force constant better (table 2 in [13]). With this potential function, it has been demonstrated that the dispersion relations of the SWNTs can be successfully reproduced with acceptable discrepancy [15, 16]. The velocity Verlet method was adopted to integrate the equation of motion with the time step of 0.5 fs.

The heat pulse was applied to a local region which consists of m consecutive unit-cells around the center of the SWNT by connecting the region to a Nose-Hoover thermostat [17, 18] kept at T_p, for a time duration of 0.4 ps (Fig. 1). The system responds to the thermostat with the relaxation time of 4 fs. After disconnecting the thermostat, the system is kept with constant total energy. As our intention is to apply and observe only the heat in the nanotube and not the stress (pressure) waves, both excitation and sampling were done in terms of the coherent molecular motions by canceling the total momentums of both the bulk and the heated region. The absence of non-thermal contribution of purely acoustic and coherent waves was confirmed by calculating the mean local velocity [11]. We consider the adiabatic condition after the heating and the coherency of the excitation to be essential to study the phenomena in the framework of heat transfer. In this sense, the methodology of the current work is non-trivially different from that of the recent demonstration of the second sound in a carbon nanotube by Osman and Srivastava [19]. In the current paper, we present the results for the temperatures (T_b, T_p) = (50 K, 1000 K). The bulk temperature T_b is above the lower limit of the kinetic region, $\alpha \propto T^{-1}$ [15], where we expect the system to be strongly anharmonic. Even so, T_b is low enough to violate the quantum limit of realistic system where the reduction of the heat capacity is significant, thus the current model system serves to highlight the classical molecular dynamics of the heat conduction. Simulations, though not presented in the current paper, were also carried out for the room temperature and qualitatively similar phenomena were observed but dimmed due to enhanced thermal phonon scattering.

The local instantaneous temperature for each unit-cell is defined through the kinetic energy as

$$T(z,t) = \frac{m}{3nk_b}\sum^{n}\left[v_x(z,t)^2 + v_y(z,t)^2 + v_z(z,t)^2\right] \quad (5)$$

with k_b as the Boltzmann constant. To compute the temperature at a z-location, the energy was averaged over a unit-cell which consists of n=20 atoms [(5,5)-SWNT]. The temperature profile was computed from ensembles of typically 40 simulations with different random initial condition in order to attenuate the noise.

The computational cell was subjected to the periodic boundary condition. Therefore, the simulation models an infinitely long SWNT with local heat pulse applied at every L, the length of the SWNT. The length L is 25 nm, long enough to acquire sufficient data before phonons collide through the periodic boundary.

3. RESULTS AND DISCUSSIONS

3.1. Observation of wavelike heat conduction

The isotherm contours shown in Fig. 2 (a) depict the overall spatio-temporal history of the temperature. Here, each contour is computed by taking ensemble averages of the data from 40 MD simulations. The picture shows how the heat supplied at the origin diffuses over the field. Figures 2 (b)-(d) show the isotherms for longitudinal, radial and circumferential components, respectively. The results of the simulations for (T_b, T_p) = (50 K, 1000 K) exhibit the heat wave of collective phonons traveling from the centered heated region of the SWNT towards the boundaries. As for the width of the perturbed cell, we performed the simulations for m=6 and 12, which resulted in a minute difference. Note that, although a wide range of wave vector components are perturbed by the pulse with width m, there should be certain distribution with the characteristic wavevector given by $\pi/\sqrt{3}a_{c-c}m$, where a_{c-c} is the interatomic distance.

The propagation characteristics of phonons can be well-understood from the dispersion relations as shown in Fig. 3. The dispersion relations can be computed by taking the two-dimensional Fourier spectra of the time history of the one-dimensional velocity field along the SWNT. Here, the results are presented as the energy density in (ω,k)-space

$$E(\omega,k)=\frac{1}{3n}\sum_{\alpha}^{3}\sum^{n}\left|\frac{1}{N}\int v_{\alpha}(z,t)\exp(ikz-i\omega t)dtdz\right|^{2}, \quad (\alpha=r,\phi,z), \tag{6}$$

where N is the number of atoms in z-direction, i.e. the number of unit-cells in the nanotube. The velocity vector is projected to the local cylindrical coordinates (r,ϕ,z) denoted by the subscript α in Eq. (6). The energy density was first computed for each directional component then summed to obtain the overall dispersion relation shown in Fig. 3. Here, k-space is normalized by the width of the Brillouin-zone of the (5, 5)-SWNT, $\pi/\sqrt{3}a_{c-c}$, and denoted with k^*. In the current case with an armchair SWNT, a unit-cell is an armchair-shaped monolayer. The data are discrete due to the finite length of the nanotube and the broadening of the spectral peaks indicates the phonon scattering. As demonstrated in [15, 16], the dispersion relation can also be computed from displacements from the equilibrium positions which, unlike the current method, would reflect the population distribution of phonons. The current method using velocity, due to the simplicity in projecting the velocity vector to the unit-cell based local cylindrical coordinates, enables us to obtain clearer view compared with the previous method for the whole energy range. Fig. 3 (a) is drawn to provide close-ups of the low frequency and wavevector regime capturing the key phonon branches; LA (longitudinal acoustic mode), TW (twisting acoustic mode), F (flexure mode [20]) together with three low frequency optical phonon branches. The sketch on the top indicates the assignment of the branches. The

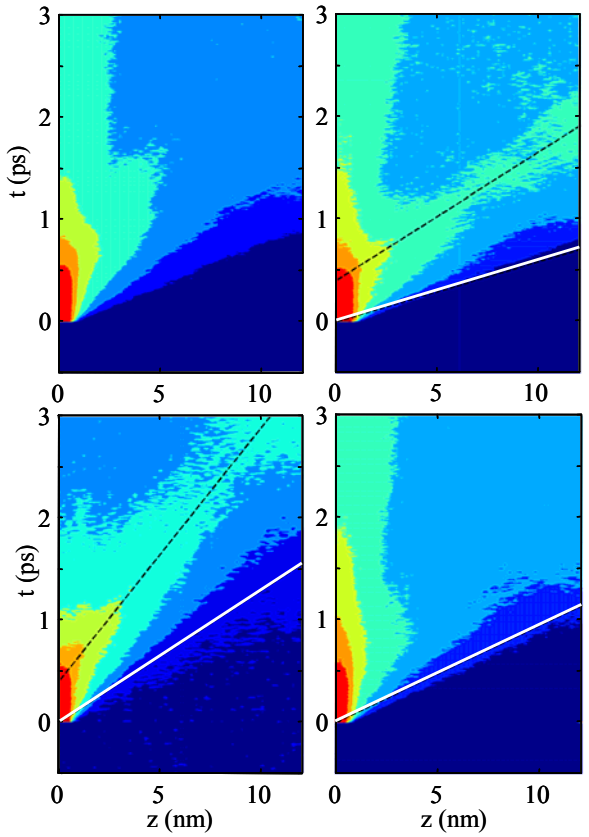

Fig. 2. Spatio-temporal isotherms of a (5,5)-SWNT subjected to a heat pulse at the origin. (a) overall temperature, (b) longitudinal component, (c) radial component and (d) circumferential component. Solid lines indicate c_D and dashed lines the propagation speed of heat waves. The temperature is logarithmically scaled for the contours. Relative scales of the contour amplitudes among the figures are arbitral. (T_b,T_p,m)=(50 K, 1000 K, 6).

value of c_D for the LA and TW can be estimated as 17 km/s and 11 km/s, respectively. As for the degenerated F branch, we compute the group velocity of the quasi-linear regime ($0.1<k^*<0.4$). Denoting this group velocity with c_D for convenience, we estimate c_D =7 km/s

In Fig. 2, the group velocity c_D is denoted with the solid lines. These long wavelength acoustic phonons travel without decaying until they collide with the counter-propagating ones through the periodic boundary, which suggests that their mean free paths are equivalent to or larger than $L/2$. The observation of fully ballistic transport of long-wavelength acoustic phonons agrees with the reported divergence of the thermal conductivity with respect to the length in the current range of tube length [15, 16]. In Fig. 2(a), an interesting feature of the contour plot is the energy transported with slower group velocity than c_D visualized as streaks stretching from near the origin to both positive and negative z-directions. The phonons forming the heat flux possess dominant energy among all the phonons, yet exhibit smaller group velocity than c_D. The decomposed isotherms [Fig. 2(b-d)] show that the observed heat wave is the superposition of heat waves of different directional components. As denoted with dashed lines, the collective phonons clearly exhibit the wavelike nature. Comparing the dimensional energy intensity of the heat waves, the radial heat wave (H_R) contains approximately double the energy of the longitudinal heat wave (H_L) and the circumferential component plays a minor role. The propagation speeds of the heat waves are c_{HL}=8 km/s and c_{HR}=4 km/s.

3.2. Comparison with macroscopic non-Fourier heat conduction equations

Now, we carry out quantitative analyses by fitting the obtained results to the Cattaneo and Vernotte's hyperbolic equation [Eq. (1)] and the dual relaxation timescale model [Eq. (2)]. As a consequence, the

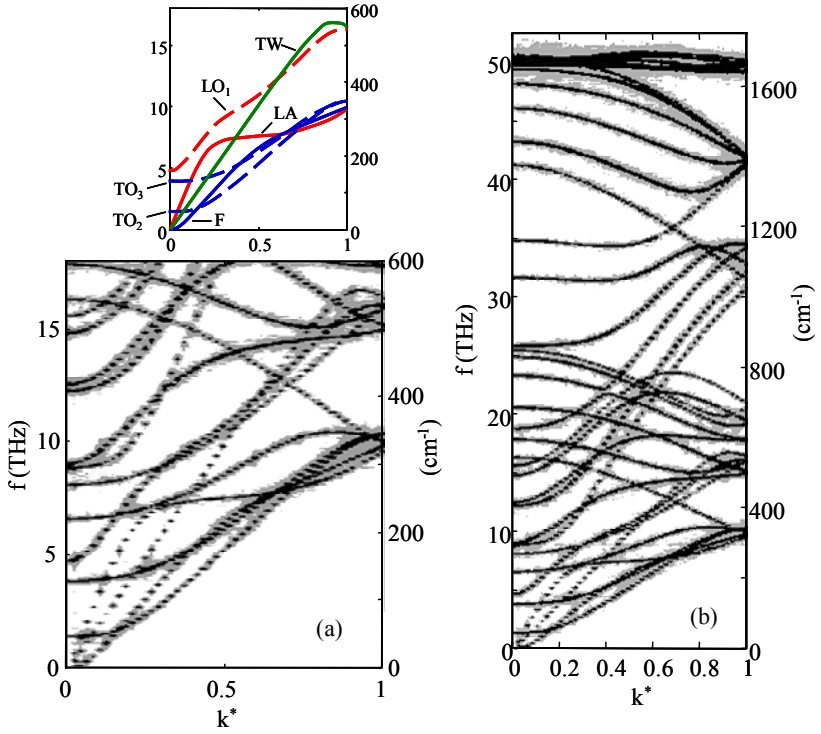

Fig. 3. Phonon dispersion relation of a 25 nm-long (5, 5)-SWNT. The dispersion relation was obtained by computing the energy density. Wavevector k^* is normalized with the Brillouin-zone width $\pi/\sqrt{3}a_{c-c}$, where a_{c-c} is the length of c-c bonds. (a) provides a focused view of (b) on the lower frequency regime. The top sketch depicts the assignments to the phonon branches: LA, TW and F indicate the longitudinal acoustic, twisting acoustic and flexure modes [20]. LO and TO indicate longitudinal and transverse optical modes. The subscript s denotes modes with sth lowest frequency (at k=0)

attempts to fit T to the equations fail due to the existence of separately conducted two major heat fluxes. In Fig. 4, longitudinal profiles of the dimensionless temperature $\theta = T/T_p$ are plotted for different time. The figure exhibits how the initial distribution (t^*=0) splits into (I) a regime with slower fully diffusive conduction and (II) a regime with faster quasi-ballistic conduction (t^*=0.32). More continuous view of the two separated heat flux is available in Fig. 2 (a) where, in addition to H_L, there is a heat flux with comparable energy propagating with negligible group velocity. As it will be shown later, this consists of the high frequency optical phonons excited by the heat pulse with broad temporal spectral band. It would be possible to capture the fully diffusive heat flux by further generalizing Eq. (2), however in order to focus on the heat flux that resides in the heat wave, instead we simply take the radial component which has the leading contribution to the overall wavelike heat conduction. In the radial component, the separation of heat flux observed for the longitudinal component does not appear. Fig. 5 demonstrates the spatio-temporal comparison of the theories and the temperature field, $\theta_r(z,t)$ computed from the radial velocity in MD simulation. As it was illustrated in the isotherm contours of the radial component [Fig. 2(c)], the simulation results show a clear deviation from the usual exponential profile predicted by the Fourier's law and the wavelike nature is observed. The solutions of both equations were obtained by numerically solving initial value problems with the periodic boundary conditions. The initial condition, $\theta_r(z,t=t_0)$ was taken from MD simulations, where t_0=0.4 ps is the time when $\theta_r(z=0,t)$ takes the maximum value. The dimensionless time is defined as $t^*=2(t-t_0)c_{HR}/L$. The dimensionless variables are denoted by asterisk hereafter and are normalized by the length scale $L/2$ and timescale $L/2c_{HR}$. The fitting carried out to minimize the mean squared error integrated over the time period of $0<t^*<0.5$, where t^*=0.5 is roughly the time when the fastest acoustic phonons crosses the periodic boundary. Note that for Eq. (1), α is given by $c_{HD}^2\tau$ hence τ is the only fitting parameter, whereas for Eq. (2), α is taken into the fitting parameter together with τ_q and τ_θ. As a consequence, we obtain τ^*=0.3, τ_q^*=0.2 and τ_θ^*=0.035, where the timescale $L/2c_{HR}$ =3.14 ps. As shown with the dotted line in Fig. 5, the hyperbolic equation [Eq. (1)] exhibits considerable deviation from the MD results (marked with circles) due to the lack of local diffusion around the peak. The fitting can be significantly improved by the additional relaxation term in Eq. (2) as seen in the solution denoted by the solid lines. At t^*~0.48, the solution of Eq. (2) near the wave front begins to deviate slightly from the MD simulation results as the wave front approaches the periodic boundary.

3.3. Modal analyses

Since the values of c_{HR} and c_{HL} extracted from the isotherm contours in Fig. 2 roughly match the relation $c = c_D/\sqrt{3}$, it is tempting to conclude that these heat waves can be considered in analog with the second sound of the low frequency acoustic modes. However, following the derivation of the Landau expression, in this quasi-one dimensional system, one would expect the speed of the heat wave to be considerably higher since the propagation speed of heat wave should scale with inverse of square root of the number of dimensions [9, 10]. Therefore, it is essential to perform modal analyses and investigate which phonons contribute to the heat wave. Considering the nanoscale length of the SWNT with the expectedly long phonon mean free path, Debye

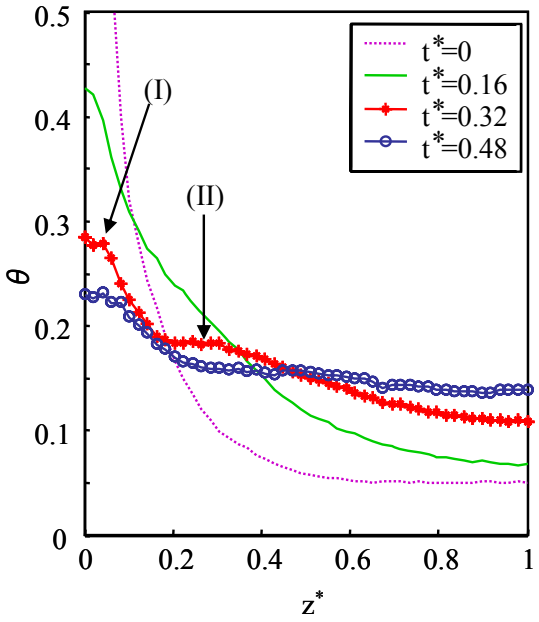

Fig. 4. The dimensionless temperature $\theta=T/T_p$ of half (positive z) of a (5,5)-SWNT at t^*=0.0, 0.16, 0.32 and 0.48 where the timescale is 3.14 ps. The arrows mark regions with (I) slower diffusive heat conduction and (II) faster non-Fourier heat conduction.

approximation may be too simple to describe the evolutions of broad phonon bands excited by the local heat pulse. On carrying out a modal analysis on such intermittent phenomena, the wavelet technique is useful as it allows us to follow the instantaneous spectrum altering in time. In contrast to the fast time Fourier transform, the wavelet transform, since the shape of the mother wavelet is frequency-invariant i.e. the timescale of the window is frequency dependent, can be tuned to capture the relaxation time that generally becomes small with increasing frequency. Here, the temporal wavelet transformation was performed on a time signal obtained from a single carbon atom using the Morlet wavelet [21],

$$\phi(f,t,\Delta t) = \exp(2\pi i f t)\exp\left[-\left(\frac{2\pi f t}{\Delta t}\right)^2\right], \qquad (7)$$

as the mother wavelet, where Δt is the characteristic width of the wavelet. The mother wavelet was chosen to possess sufficient frequency localization and symmetry. By repeatedly performing the transformation for all the carbon atoms, one can obtain temporal spectra of each velocity component for the entire spatio-temporal field.
Consequently, we define the spectral temperature as,

$$\theta_p(f,z,t) = \frac{1}{n}\sum_i^n \left[P(f,z,\phi_i,t) - P_0(f)\right]. \qquad (8)$$

The power spectrum P is ensemble averaged value of 10 numerical experiments and P_0 denotes the spectrum at equilibrium. The data are averaged over a unit-cell with n molecules to project the spectrum to the one-dimensional space.

In figures 6 and 7, the results are presented as temporal sequences of spectral contours in the (f,z)-field for longitudinal and radial components, respectively. The input heat pulse excites a wide range of frequency components. Note that since the nanotube is initially excited to a strongly non-equilibrium state, the phonon population is far off the statistical phonon distribution at equilibrium. Such state with high phonon populations in the high frequency optical branches can also be observed on subjecting a nanotube to optical excitations. The receptivity of an SWNT to the local excitation reflects the phonon density of state of the nanotube. As a consequence, for instance for the longitudinal component, major energy is distributed to the band around 50 THz, an optical phonon branch of the in-plane lattice vibration [15, 16]. However, due to the small group velocities of the phonons in this band, the heat flux hardly propagates and merely diffuses at around z=0. This is in fact the main contributor to the fully diffusive heat flux with negligible group velocity observed in Fig. 2(a). On the other hand, in a broad range of lower frequency in both longitudinal and radial components (Fig. 6 and 7), there are energy fluxes that show distinct propagation, which is best observed in the local spectral peaks detaching from the center (z=0) and traveling toward the boundary. The trend is most evident in the distinct energy around 9 THz in the radial component (Fig. 7), which corresponds to the band of large local density of states [15, 16]. The propagation speed of the band peak, marked with triangles in the figure, was found to correspond with c_{HR}. The peak frequency, 9THz, approximately corresponds to the frequency of the transverse acoustic phonons at the Brillouin-zone boundary, and since phonons with such short

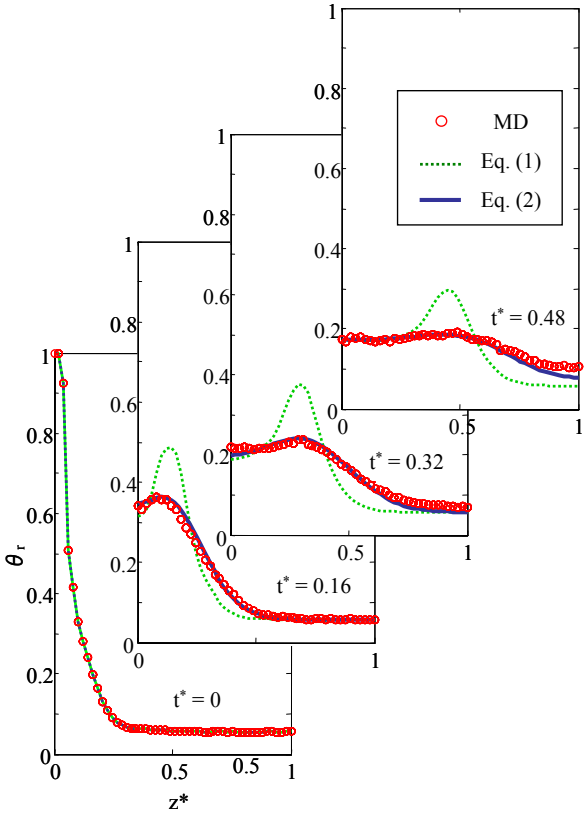

Fig. 5. Temporal sequences of the dimensionless temperature profile of H_R. Circles: MD results. Dotted lines: The hyperbolic wave equation [Eq. (1)] with τ*=0.3. Solid lines: dual time scale equation [Eq. (2)] with τ_q*=0.2 and τ_θ*=0.035.

wavelength can be considered to carry minute heat, the major energy of the present heat wave should reside in the transverse optical phonons. These wavelet transformed spectra also serve to visualize various channels of phonon band to band energy transport. For instance, in Fig. 6, an energy transport channel from the high frequency band of the in-plane lattice vibration (~50 THz) to lower frequency bands can be observed. The relatively long tail of the energy transport of longitudinal phonons around 18 THz suggests that there is energy feed from other frequency bands, presumably the above mentioned phonons of the in-plane lattice vibration.

The current results show that the optical phonons may play a significant role in non-Fourier heat conduction of carbon nanotubes subjected to local coherent phonon excitations. The optical phonons are usually considered to be poor heat carrier in bulk heat conduction due to their relatively small group velocity in long wavelength regime and small relaxation time. However, the dispersive relations of the SWNT show that, in intermediate range of the normalized wavevector $0.1<k^*<0.9$, some of the phonon branches, especially the ones with relatively low frequency, have group velocity comparable to the acoustic branches. Unfortunately, the current analysis does not allow us to detect the spatial mode of the heat flux, hence we are not able to specify or weigh the contributions from certain phonon branches. Nevertheless, with the sufficiently high group velocity together with the relatively large relaxation time due to the quasi-one-dimensional structure, the heat conduction length-scale of optical phonons, $c\tau$, falls in the order of the realistic length of SWNTs in actual application devices.

It is worth noting that there is certainly energy in the low frequency acoustic modes excited by the heat pulse. As mentioned above, they form the transport front of the heat flux in each directional component. Although these phonons are expected to dominate the heat conduction of longer carbon nanotube due to their large relaxation time and group velocities, the modal analyses show that these phonons do not contribute to the visible collective phonon transport observed in the current SWNT with relatively short length. Judging from the observation that these phonons exhibit fully ballistic transport, it is possible that the lower limit of the second sound criteria $\tau_N<t$ [7] was not satisfied for these phonons, i.e. there is not sufficient normal phonon scattering to sustain the

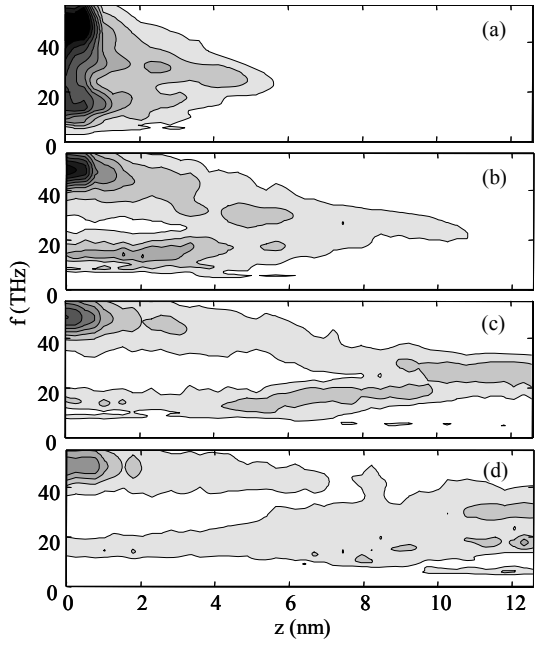

Fig. 6. Temporal sequence of spectral temperature computed by wavelet transformations $\theta_p(f,z,t)$ of longitudinal velocity component. Figures (a-d) denote the spectra at (a) t^*=0.032, (b) 0.25, (c) 0.48 and (d) 0.73.

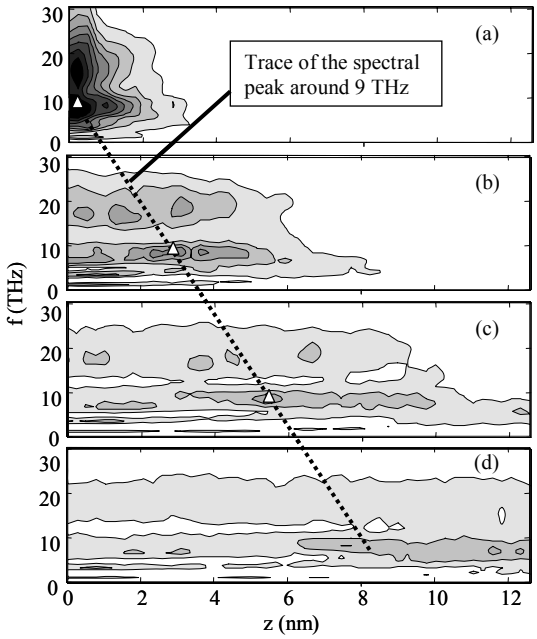

Fig. 7. Temporal sequence of spectral temperature computed by wavelet transformations $\theta_p(f,z,t)$ of radial velocity component. Figures (a-d) denote the spectra at (a) t^*=0.032, (b) 0.25, (c) 0.48 and (d) 0.73. Note that the current frequency range (~30THz) captures the entire energy range for the radial component [15, 16].

connection between phonons as a collective waves. If this is the case, there is a possibility to observe heat waves based on low frequency acoustic phonons in system by either increasing the system timescale or decreasing τ_N. This can be realized by simulating longer nanotubes or under higher temperature, respectively.

4. CONCLUSIONS

The non-Fourier heat conduction was investigated in SWNTs subjected to a local heat pulse with time duration of sub-picoseconds, using molecular dynamics simulations. In the system with quasi-one-dimensional thermal properties, we have demonstrated that the distinct heat flux is conducted in a wavelike form. The evolution of the wavelike propagating heat flux can not be predicted by the convectional hyperbolic wave equation due the influence of the local diffusion. This essence can be captured by the taking dual relaxation timescale into account. The results show that the spatio-temporal evolution of the wavelike heat conduction in the SWNT with nanoscale length can be well described by the phenomenological macroscopic relation. The modal analyses using wavelet transformations show that the major contribution to the wavelike heat conduction comes from the optical phonon modes with sufficient group velocity and probably with wave vectors in the intermediate regime.

ACKNOWLEDGEMENT

The work is supported in part by the Japan Society for the Promotion of Science for Young Scientists and KAKENHI #17656072

REFERENCES

1. D. D. Joseph and L. Preziosi, Rev. Mod. Phys. **62**, 375 (1990)
2. P. Vernotte, C. R. Acad. Sci. **246**, 3154 (1958)
3. C. Cattaneo, C. R. Acad. Sci. **247**, 431 (1958)
4. D. Y. Tzou, ASME J. Heat Transfer **117**, 8 (1995)
5. D. W. Tang and N. Araki, Int. J. Heat Mass Transfer **42**, 855 (1999)
6. E. W. Prohofsky and J. A. Krumhansl, Phys. Rev. **133**(5A), A1403 (1964)
7. R. A. Guyer and J. A. Krumhansl, Phys. Rev. **148**, 766 (1966)
8. L. Landau, J. Phys. U.S.S.R. **5**, 71 (1941)
9. M. Chester, Phys. Rev. **131**(5), 2013 (1963)
10. D. H. Tsai and R. A. MacDonald, Phys. Rev. B **14**(10), 4714 (1976)
11. S. Volz, J. B. Saulnier, M. Lallemand, B. Perrin, P. Depondt and M. Mareschal, Phys. Rev. B **54**, 340 (1996)
12. S. T. Huxtable, D. G. Cahill, S. Shenogin, L. Xue, R. Ozisik, P. Barone, M. Usrey, M. S. Strano, G. Siddons, M. Shim and P. Keblinski, Nature Mat. **2**, 731 (2003)
13. D. W. Brenner, Phys. Rev. B **42**, 9458 (1990)
14. Y. Yamaguchi and S. Maruyama, Chem. Phys. Lett. **286**, 336 (1998)
15. S. Maruyama, Physica B **323,** 272 (2002)
16. S. Maruyama, Micro. Therm. Eng. **7**, 41 (2003)
17. S. Nose, J. Chem. Phys. **81** (1), 511 (1984)
18. W. G. Hoover, Phys. Rev. A **31**, 1695 (1985)
19. M. A. Osman and D. Srivastava, Phys. Rev. B **72**, 125413 (2005)
20. G. D. Mahan and G. S. Jeon, Phys. Rev. B **70**, 075405 (2004)
21. C.Torrence and G.P.Compo, Bull. Amer. Meteor. Soc., **79**, 61 (1998)